



Copper-cyclodextrin metal-organic framework as a green catalyst for the thermal decomposition of nitrocellulose

Yameng Chai^{a,b}, Wenjia Li^{a,b}, Fuqiang Du^c, Jianchun Zhao^c, Shiying Li^{a,b}, Yajun Ding^{a,b}, Sanjiu Ying^{a,b}, Jie Zhou^{a,b,*}

^a School of Chemistry and Chemical Engineering, Nanjing University of Science and Technology, Nanjing 210094, China

^b Key Laboratory of Special Energy Materials of Ministry of Education, Nanjing University of Science and Technology, Nanjing 210094, China

^c Lu Zhou North Chemical Industries Co. Ltd., Luzhou, China



ARTICLE INFO

Keywords:

Cyclodextrin
Metal organic framework
Nitrocellulose
Catalytic activity
Decomposition mechanism

ABSTRACT

Copper-cyclodextrin metal-organic framework (Cu-CD-MOF) prepared via the vapour diffusion method was applied as an environmentally friendly catalyst for the pyrolysis process of nitrocellulose (NC). The structural and thermal properties of Cu-CD-MOF were comprehensively and meticulously characterized. Differential scanning calorimetry results disclosed the good compatibility of Cu-CD-MOF toward NC. The NC/Cu-CD-MOF mixture exhibited a decrease of 21.6 KJ/mol in energy barrier, which was resulted from the catalytic characteristics. The TG-FTIR measurement confirmed the maximum pyrolysis rate temperatures of NC/Cu-CD-MOF mixture was decreased by 0.9 °C than NC. Furthermore, Cu-CD-MOF was able to accelerate the rupture of the -O-NO₂ bond and the secondary self-catalytic reaction. The toxic and harmful gas concentrations were also reduced. This work provided a new path to design green catalysts for NC-based materials.

1. Introduction

Nitrocellulose (NC) has high flammability, special mechanical strength, low cost, and compatibility with various additives, serving as one of the most commonly used energy components in propellants and explosives [1-4]. There has been a relentless pursuit of developing novel catalysts designed to regulate the thermal property of NC, ultimately enhancing the overall performance of NC-based composites. They not only meticulously control the decomposition and combustion at the microscale but also optimize the energy release and overall safety by adjusting kinetic parameters. Therefore, the introduction of catalysts not only satisfies high-performance demands but also lays a solid foundation for the application of NC-based materials in a broader range of fields [5-9].

Due to the special electronic structure and active site formation of transition metals (iron, copper, cobalt, etc.), transition metals have received much attention in catalysing NC-based composite [10-13]. Amongst transition metals derivative materials, metal-organic frameworks (MOFs) possess flexible structure, high porosity, and rich diversity [14,15], which have been widely applied in the catalytic field [16-18]. On this basis, MOFs with transition metals such as Fe, Cu, and

Co are being ever-increasingly fascinating catalysts for NC applications. Wang et al. synthesized a Cu-MOF composite with reduced graphene oxide as a high-energy combustion catalyst. They found that Cu-MOF@CNT-rGO has good catalytic ability and can reduce the peak temperature of AP's high-temperature thermal decomposition by about 100 °C [19]. Yang et al. synthesized a novel three-dimensional solvent-free energetic MOF ([Pb(HBTI)]_n) that combines two exothermic peaks of AP into a broad peak, and the peak temperature is reduced to 313 °C, much lower than the exothermic peak temperature of AP (335 °C) [20]. However, such MOFs are made from azoles, azines, and benzene ligands, which have a certain toxicity and can impact the environment during production and processing [21].

In recent years, "biological MOFs" utilizing biomolecules as organic ligands feature non-toxic, environmentally friendly, and easy to recycle. Especially, cyclodextrin (CD)-based MOFs have attracted intensive attention and have shown broad application prospects in multiple fields [22-25]. However, research on natural green MOFs as catalysts for high-energy materials has not been reported yet. In this contribution, Cu-CD-MOF was synthesized through a typical diffusion method. For comparison, its carbonization derivative (Cu-CD-MOF-NPC) was further prepared by a high-temperature calcination. The thermal decomposition

* Corresponding author.

E-mail address: fnzhoujie@njust.edu.cn (J. Zhou).

temperature, and activation energy of NC-based composites (NC/Cu-CD-MOF and NC/Cu-CD-MOF-NPC), which were evaluated by using differential scanning calorimetry (DSC). TG-FTIR was employed to detect the generated gases or fragments and derive to the possible catalytic mechanism of Cu-CD-MOF. The insights gained from this study can provide guidance for the development of novel, extremely reliable, and highly active biological MOFs-based catalysts for their application in the field of energetic materials.

2. Experimental section

2.1. Materials

β -Cyclodextrin (β -CD, 98%) was purchased from Tokyo Chemical Industry (TCI, Japan). Copper chloride (Mol. Wt. 170.48 g/mol) ($\text{CuCl}_2 \cdot 2\text{H}_2\text{O}$), anhydrous methanol (MeOH, 99.8%), and anhydrous ethanol (EtOH, 99.7%) were purchased from Sigma-Aldrich (St. Louis, MO, USA). Nitrocellulose (nitrogen content: 12.10 wt.%) was provided by Luzhou North Chemical Industries Co., Ltd. (Luzhou, China). All the chemical reagents were used without further purification. The deionized water was purified through a Millipore system for all experiments here.

2.2. Methods

2.2.1. Synthesis of Cu-CD-MOF

It is synthesized based on previous research reports [26]. Firstly, apply 1 mmol of β -CD in a 15 ml beaker and stir at room temperature for 20 min. Then, add 5 mL of ethanol to the stirred solution and continue stirring to make the mixture a transparent and colourless solution. Prepare a 5 mmol copper chloride solution in another beaker and stir for 10 min. Mix the metal aqueous solution with the CD solution, then inject the mixture into a large beaker containing 100 mL of methanol and allow its vapour diffusion for 5–7 days. Pour out excess solution, filter and extract Cu-CD-MOF crystals, rinse multiple times with methanol, and then dry overnight in a 60 °C oven (Fig. 1a).

2.2.2. Preparation of Cu-CD-MOF derived carbon (Cu-CD-MOF-NPC)

Place the prepared Cu-CD-MOF into a tubular carbon furnace, heat it from 30 °C to 650 °C at a heating rate of 5 °C/min in an N_2 atmosphere, then calcine it for 5 h, and finally cool it to room temperature to obtain Cu-CD-MOF-NPC (Fig. 1b).

2.2.3. Preparation of NC-based composites

At room temperature, a physical mixture of Cu-CD-MOF, Cu-CD-MOF-NPC, and NC was prepared in a grinding bowl, ensuring that the catalyst comprised 5% of the total mixture. Additionally, to test the compatibility of additives with NC, we also prepared NC-based composite materials with a mass ratio of 1:1. The grinding process is maintained for 30 min to obtain NC/Cu-CD-MOF and NC/Cu-CD-MOF-NPC composite materials (Fig. 1b).

3. Results and discussions

3.1. Structural characterization and elemental analysis

To investigate the participation of functional groups capable of reacting, FTIR spectra were performed on β -CD and Cu-CD-MOF. It is evident that the characteristic peak of β -CD is present in the infrared spectrum of the synthesized Cu-CD-MOF material (Fig. 2a). The absorption bands of functional groups are summarized in Table S1. The FTIR spectrum of pure β -CD is consistent with reference [27]. The stretching vibration of the OH group appears at 3400–3200 cm^{-1} , and exhibits a maximum peak at 3300 cm^{-1} . In the spectrum of the β -CD, the characteristic peak at 2910 cm^{-1} is due to the stretching vibration of the C—H bond. The characteristic peak at 1640 cm^{-1} is a bending vibration of the O—H bond formed due to the presence of H_2O . Intense peaks were observed at 1150 cm^{-1} (C—O) and 1020 cm^{-1} (C—O—C), while at 853 cm^{-1} it was attributed to (C—C vibrations) [28,29]. The FTIR spectrum of Cu-CD-MOF exhibits bands at 3310 cm^{-1} (O—H), 2980 cm^{-1} and 2900 cm^{-1} (C—H), and 1650 cm^{-1} (H—O—H). The stretching band of CH_2 group (2820–3030 cm^{-1}) was observed to narrow in Cu-CD-MOF, which is related to the molecular conformational changes after the formation of metal-cyclodextrin bonds [30]. It is worth noting that the peak intensity

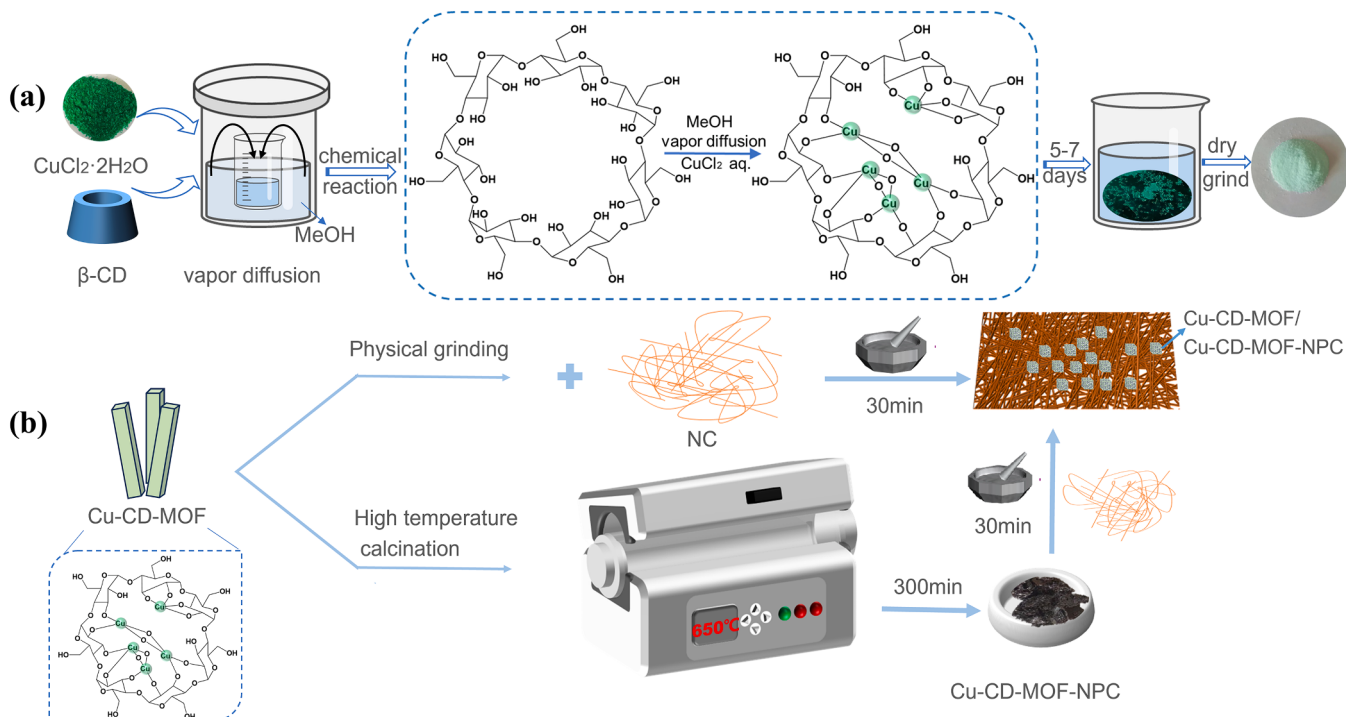


Fig. 1. (a) The actual reaction for generating Cu-CD-MOF. (b) Preparation of NC-based composite materials (above) and Cu-CD-MOF-NPC (below).

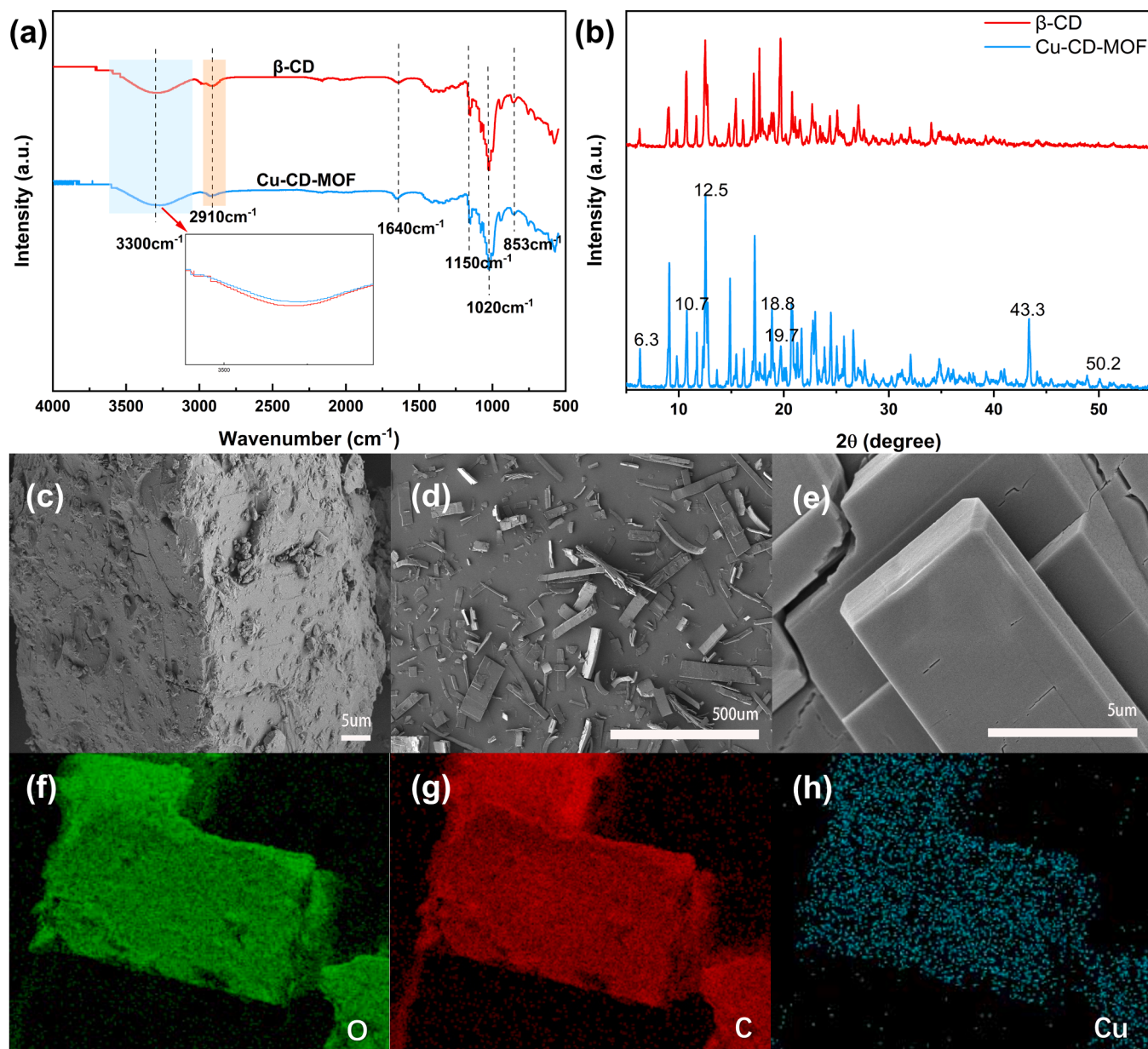


Fig. 2. FT-IR spectra (a) and Powder X-ray diffraction patterns (b) of β -CD and Cu-CD-MOF. (c) SEM image of the β -CD. (d) and (e) SEM images of the Cu-CD-MOF. (f)-(h) The elemental distribution mapping images of the Cu-CD-MOF.

of O—H groups in the synthesized material is reduced relative to β -CD, indicating the presence of CD and copper in the crystal [31,32]. Therefore, by comparing FTIR spectra of β -CD and Cu-CD-MOF, it was found that cyclodextrin exists in the synthesized Cu-CD-MOF, which is consistent with previous CD-MOFs [28].

The crystal structure of the prepared Cu-CD-MOF was characterized using XRD (X-ray diffraction) analysis, and the diffraction pattern is shown in Fig. 2b. Based on the provided information, the X-ray diffraction pattern of Cu-CD-MOF shows a correlation with β -CD, suggesting the coupling of CD as an organic linker [30]. A high-intensity peak was observed in Cu-CD-MOF, which differs from the peaks seen in β -CD. The diffraction peaks of β -CD are at 10.8° , 12.1° , 18.5° , and 19.7° , while the diffraction peaks of Cu-CD-MOF are observed at 6.3° , 10.7° , 12.5° , 18.8° , 19.7° , 43.3° (111), and 50.2° (200). These new diffraction peaks can be attributed to copper ions based on the standard diffraction of copper (JCPDS: Card 04-0836) [33]. The results suggest that Cu-CD-MOF has high crystallinity, consistent with previous studies [26], and confirm the presence of β -CD and copper, in line with other

β -CD-MOF XRD spectra [34].

To explore the distribution of elements and the morphology of materials, we used scanning electron microscopy (SEM) and energy-dispersive X-ray spectroscopy (EDS). This analytical method can identify the compositional elements present in the synthesized product. The SEM image of the cyclodextrin and copper ion-modified porous organic framework (Cu-CD-MOF) sample is shown in Fig. 2c&d. It can be seen that the SEM image of cyclodextrin shows particles with irregular and non-smooth structures. On the other hand, the SEM image of the prepared MOF (Fig. 2d) shows a crystal shape with a rodlike structure with regular and rough surfaces. Elemental mapping results (Fig. 2f-h) indicate the presence of copper (Cu) element, in addition to the carbon (C) and oxygen (O) elements of cyclodextrin itself. Furthermore, the uniform distribution of C, O, and Cu elements throughout the sample confirms the successful synthesis of the MOF.

Furthermore, we conducted a detailed observation of the morphology of the NC-based composite material using SEM (Fig. S1). The SEM images clearly reveal that the catalyst particles are uniformly

dispersed around the nitrocellulose (NC), with no significant agglomeration observed. Analysis of the element distribution map confirms that the catalyst elements exhibit a uniform distribution on the surface of the nitrocellulose (NC), strongly demonstrating the good dispersion and homogeneity of the catalyst within the NC-based composite material.

Fig. S2 displays the nitrogen adsorption and desorption isotherms, along with the pore size distribution curves, of Cu-CD-MOF. The isotherm diagram of Cu-CD-MOF shows a type I isotherm with a microporous structure, and the pore diameter is concentrated at 1.27 nm. The pore size of Cu-CD-MOF-NPC is mostly distributed in large pores, which are significantly larger than that of Cu-CD-MOF. Using the BET equation, the specific surface area of Cu-CD-MOF was determined to be 381.423 m²/g. Its large specific surface area and porous structure provide more active sites for gas enrichment and catalytic pyrolysis.

Cu-CD-MOF was heated at a heating rate of 10 °C/min in the N₂ atmosphere, and the temperature range of the TGA curve is between 50 °C and 800 °C. Cu-CD-MOF exhibits significant degradation at 220.0–300.0 °C. Compared to the decomposition temperature of β-CD at 350.0 °C [35], Cu-CD-MOF exhibits lower thermal stability during metal ion insertion. This is due to the weaker metal distribution nodes and the formation of porous structures reducing thermal stability, which is consistent with previous research results [36–38]. Cu-CD-MOF exhibits a two-step degradation process, with approximately 5% weight loss occurring at around 220 °C due to the breaking of the bond bridge between Cu and cyclodextrin. Between 270 and 325 °C, approximately 60% of Cu-CD-MOF experiences significant weight loss due to MOF skeleton collapse [35,39,40]. Additionally, the analysis of the DTG curve of Cu-CD-MOF showed that the degradation temperature of Cu-CD-MOF reached 222.5 °C (**Fig. 3a**) which is lower than the decomposition temperature of β-CD (300.0–350.0 °C) [35]. This indicates that with the introduction of Cu, the degradation temperature decreased, thereby affecting the thermal stability of the structure. Moreover, DSC curve analysis shows that the stability of Cu-CD-MOF is lower than that of β-CD, with β-CD having a peak endothermic temperature of 324.9 °C. The two endothermic temperature ranges of Cu-CD-MOF correspond to its TGA decomposition stages, further confirming the successful preparation of Cu-CD-MOF.

This study comprehensively characterized the intricate structure and properties of Cu-CD-MOF through a multifaceted analytical approach. FTIR spectroscopic analysis revealed the functional groups present in Cu-CD-MOF and β-CD, confirming the formation of chemical bonding. XRD analysis demonstrated the crystalline structure of Cu-CD-MOF and verified the presence of copper ions. Furthermore, SEM and EDS investigations delved into the material's morphology and elemental composition, revealing a well-ordered rod-like structure with a uniform distribution of copper, carbon, and oxygen. Notably, TGA analysis indicated a reduced thermal stability in Cu-CD-MOF, a finding coherent

with the anticipated decrease in thermal decomposition temperature owing to the incorporation of copper. BET analysis then quantified the material's specific surface area and pore size distribution, underscoring its impressively large surface area and microporous framework. By integrating the results from these techniques, we were able to comprehensively characterize the structure and properties of Cu-CD-MOF, providing strong support for its potential applications in catalysis, adsorption, and other fields.

3.2. Thermal analysis

During the preparation of energetic composite materials, additives may react with high-energy compounds, affecting the storage life and safety of the materials. Compatibility is a critical safety factor in assessing the manufacturing and storage of energetic materials, and a lack of compatibility may lead to spontaneous combustion or explosion. Therefore, studying the compatibility of additives with energetic materials is crucial for the development of new energetic materials [41–43]. Due to its time-saving, small sample size, easy operation, and safety, differential scanning calorimetry (DSC) has become a popular method for evaluating explosives and additive compatibility [44]. **Table S2** shows the compatibility evaluation criteria for propellants and additive materials. The DSC heat flux curves of NC, NC/Cu-CD-MOF (1:1) and NC/Cu-CD-MOF-NPC (1:1) at heating rates of 2, 5, 10, and 20 °C/min are shown in **Fig. 4**. The change in decomposition peak temperature of NC/Cu-CD-MOF and NC/Cu-CD-MOF-NPC mixed system compared to NC alone is ±2.0 °C. This result shows good compatibility between Cu-CD-MOF, Cu-CD-MOF-NPC and NC (grade A). In addition, their thermal safety parameters were calculated according to **Eqs. S(1)–(3)**, which is of great significance for further studying the thermal stability of high-energy materials and their sensitivity to mechanical stimuli. The calculation results are shown in **Table. S3**. The parameter values of NC/Cu-CD-MOF and NC/Cu-CD-MOF-NPC have relatively small changes compared to NC, indicating that both can be added to NC for use. Therefore, Cu-CD-MOF and Cu-CD-MOF-NPC materials can be used as components for preparing propellants.

In this study, we characterized the thermal properties of NC, NC/Cu-CD-MOF, and NC/Cu-CD-MOF-NPC through Differential Scanning Calorimetry (DSC) (**Fig. 4d**). As can be observed from **Fig. 4d**, both NC and NC-based composite materials exhibit a single exothermic peak during the thermal decomposition process, corresponding to the breaking of -O-NO₂ bonds in NC thermal decomposition, followed by a self-catalytic parallel reaction [45–47]. At a heating rate of 10.0 °C/min, the peak temperature of NC thermal decomposition is 209.1 °C, which is very close to the value reported in the literature (209.2 °C) [48]. However, after being compounded with Cu-CD-MOF and Cu-CD-MOF-NPC, the exothermic peak temperatures decrease to 206.8

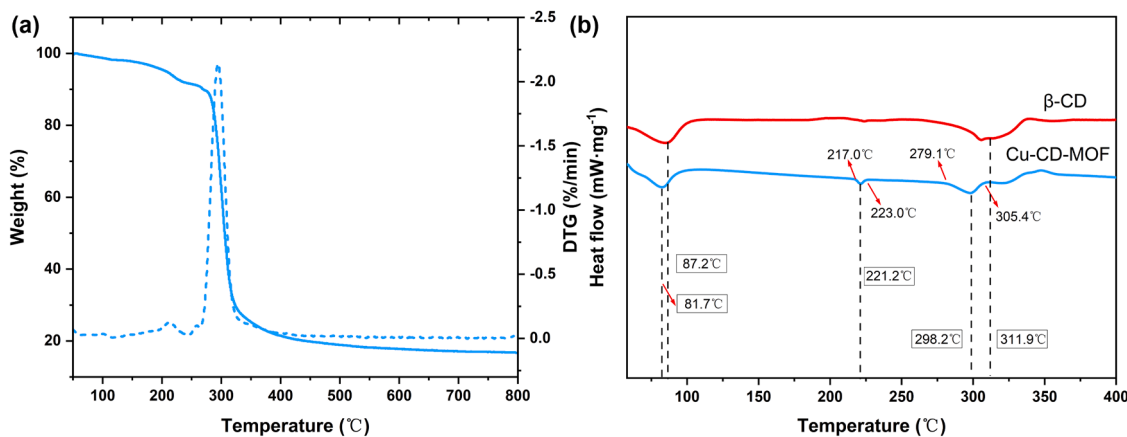


Fig. 3. (a) TG and DTG curves of Cu-CD-MOF (b) DSC curves of β-CD and Cu-CD-MOF.

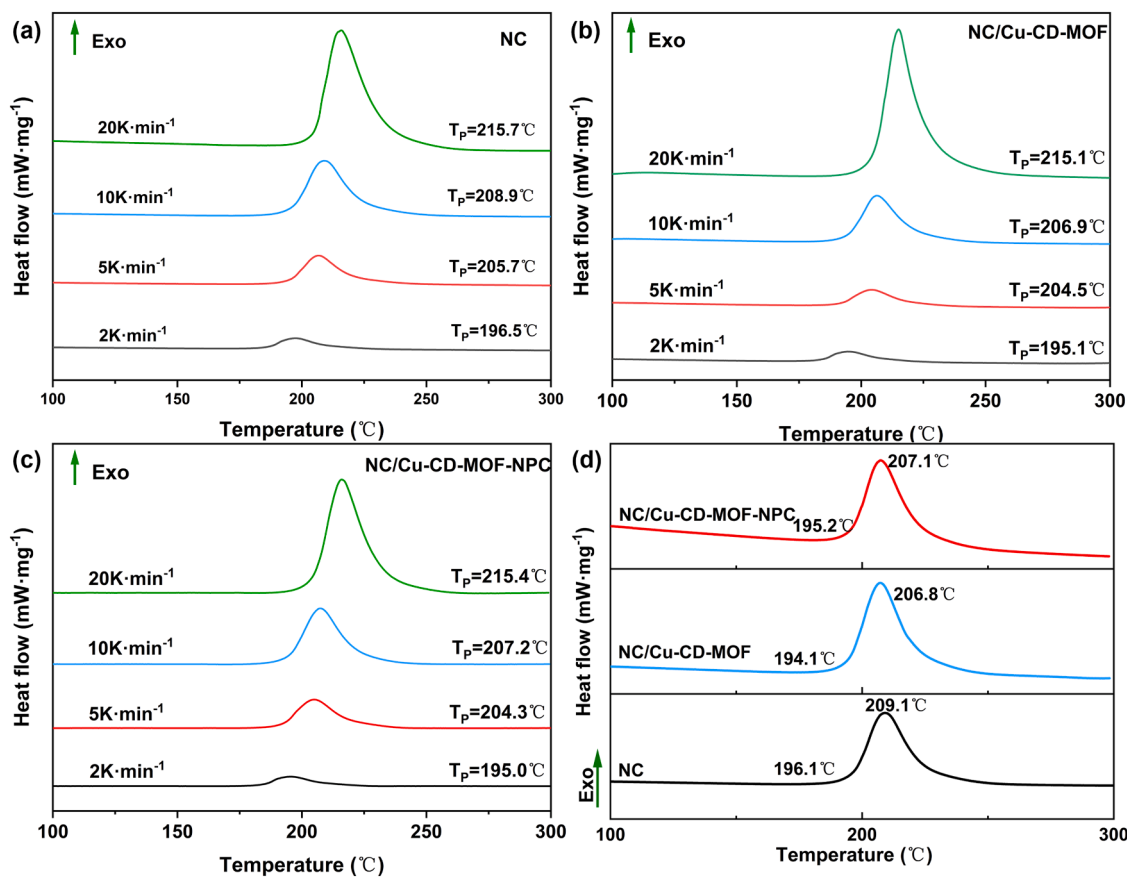


Fig. 4. (a)-(c) DSC curves of NC, NC/Cu-CD-MOF (1:1) and NC/Cu-CD-MOF-NPC (1:1) obtained at a heating rate of 2, 5, 10, 20 °C/min. (d) DSC curves of NC, NC/Cu-CD-MOF (catalyst content 5%) and NC/Cu-CD-MOF-NPC (catalyst content 5%) obtained at a heating rate of 10 °C/min.

°C ($\Delta T=2.3$ °C) and 207.1 °C ($\Delta T=2.0$ °C), respectively. This indicates that the introduction of copper-based coordination polymers reduces the thermal stability of NC. The DSC curves of analogous materials reported in the literature exhibit a comparable trend. To evaluate the thermal performance of the materials, we compared our DSC curves with those of similar materials from existing literature (Table S5). By comparing with the most advanced curves available, the study validates the catalytic effectiveness of Cu-CD-MOF and Cu-CD-MOF-NPC as NC-based composite materials, offering broader prospects for their practical applications.

3.3. Kinetic parameter, physical model and kinetic compensation effects

The complexity and randomness of polymers give rise to diverse reactions. To tackle this issue, kinetic modelling is crucial in tracking the reaction histories of both individual and lumped species. Most of the kinetic parameters for polymer degradation are derived from experiments that reflect overall kinetics, making them inherently lumped in nature. This is particularly evident from previous studies that have found significant variations in the kinetic parameters for poly(methyl methacrylate) (PMMA) thermal degradation. Therefore, the E_a values obtained from thermal analysis experiments represent the apparent parameters or overall kinetics of these reactions, reflecting the complexity and randomness inherent in polymer degradation reactions [49].

Based on DSC curve data with a linear heating rate, the thermal decomposition kinetics of NC and NC-based composites were studied using the Flynn-Wall-Ozawa (FWO) equation [50], the Kissinger-Akahira-Sunose (KAS) equation [51], and the Friedman equation [52]. The kinetic parameters of NC and NC-based composites were determined using the FWO method, KAS method, and Friedman

method based on the relationship curve between reaction conversion (α) rate and temperature (T) (Fig. S3).

The E_a values (including the corresponding confidence intervals) of NC and NC-based composites and the relation curve of reaction conversion rate are obtained from the analysis of the above three models, as shown in Fig. 5. For pure NC, as α varies within the range of 0 to 0.9, there emerges a discernible upward trend in the E_a value as the thermal process ensues. But the results showed that the E_a value of NC/Cu-CD-MOF first slowly increased and then decreased with the increase in conversion rate. The E_a value of NC/Cu-CD-MOF-NPC shows a gradual increase when the conversion rate is 0–0.85, and then gradually decreases with the increase in the conversion rate. Remarkably close E_a values are obtained for the same samples when utilizing the FWO and KAS methods, however, the discrepancies between the E_a obtained using Friedman's method and those calculated by the other two approaches may be attributed to the accuracy of the derivative of mass loss [53,54]. Compared to pure NC, the E_a values of NC/Cu-CD-MOF and NC/Cu-CD-MOF-NPC were significantly reduced.

The activation energies of the three models are listed in Table S4. The E_a values of pure NC by FWO method, KAS method, and Friedman method are 182.2, 182.1, and 196.1 kJ/mol. The average activation energy of NC calculated using the above three methods is 186.8 kJ/mol, which is close to the values reported in previous studies [55]; Whereas the E_a values of the NC/Cu-CD-MOF composite are 174.6, 174.5, and 177.9 kJ/mol, respectively. The average E_a values of NC/Cu-CD-MOF-NPC composite materials are slightly higher than those of NC/Cu-CD-MOF at 176.8, 176.4 and 188.7 kJ/mol, respectively.

The average E_a values of NC, NC/Cu-CD-MOF and NC/Cu-CD-MOF-NPC composites fall within a range typical for the thermal kinetics of energetic materials (with E_a ranging from 80 to 250 kJ/mol). Based on the data provided, the average E_a of the NC/Cu-CD-MOF and NC/Cu-CD-

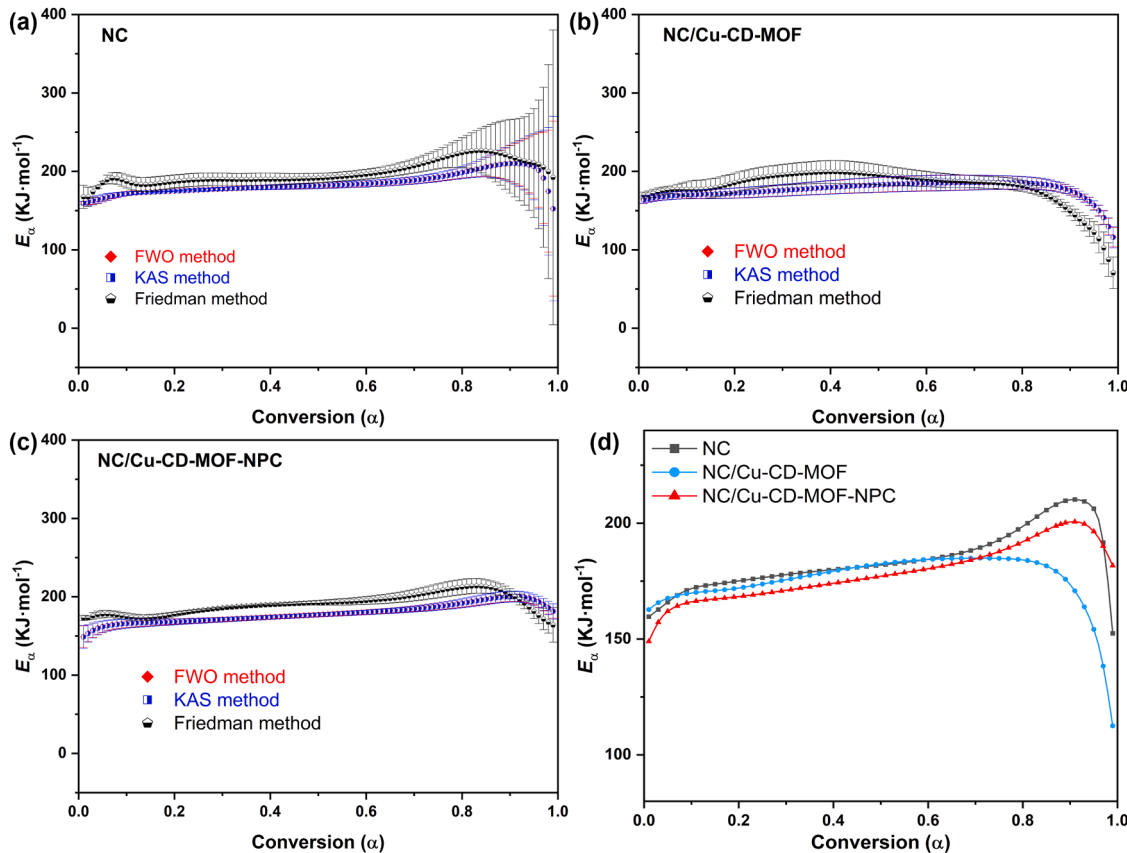


Fig. 5. (a)–(c) E_α - α curves of NC and NC-based composites calculated by FWO, KAS and Friedman methods. (d) E_α - α curves of NC and NC-based composites by Flynn-Wall-Ozawa's method.

MOF-NPC composites is reduced by up to 21.6 and 19.7 kJ/mol compared to the average E_α of NC. This explains the catalytic effect of Cu-CD-MOF and Cu-CD-MOF-NPC on the thermal decomposition of NC.

To verify the accuracy of E_α , the thermal degradation kinetics of NC, NC/Cu-CD-MOF, and NC/Cu-CD-MOF-NPC were calculated using the Kissinger method (Eq. S(4)) and the Ozawa method (Eq. S(5)), based on experimental data of thermal decomposition peak temperatures and heating rates of pure NC, NC/Cu-CD-MOF, and NC/Cu-CD-MOF-NPC. By applying Eq. S(4) and Eq. S(5), corresponding scatter plots for each model can be plotted and fitted (Fig. S4), with regression correlation coefficients greater than 0.997. The activation energies of NC, NC/Cu-CD-MOF and NC/Cu-CD-MOF-NPC thermal degradation processes were calculated using two models. From Fig. S5, it can be seen that the activation energies obtained by two models are basically the same. The similarity of the activation energy values obtained based on the Ozawa and Kissinger models can prove the accuracy of the experimental results. Additionally, the activation energies of NC/Cu-CD-MOF and NC/Cu-CD-MOF-NPC are lower than those of pure NC, indicating that NC/Cu-CD-MOF and NC/Cu-CD-MOF-NPC have a catalytic effect on NC.

3.4. TG-FTIR analysis

Traditional thermal analysis techniques alone are insufficient to identify the gases generated during the heating process of materials. For studying the decomposition process of high-energy materials, this information is crucial for elucidating and understanding the relevant mechanisms. The hyphenated method, which combines thermogravimetric analysis and Fourier transform infrared (TG-FTIR), can track the release of gases during the thermal decomposition process in real time, test the thermal decomposition behaviour of energy materials more accurately, and infer the decomposition mechanism. Consequently, TG-

FTIR has garnered widespread attention in the field of high-energy materials research. The application of TG-FTIR is not only beneficial for comprehensively understanding the decomposition behaviour of energetic materials but also for facilitating the development of newer and safer energetic materials [56].

Based on this, the thermal decomposition process of NC and NC-based composite materials was investigated using TG-FTIR. Fig. S6 exhibits the TG-DTG curves within the temperature range of 50–400 °C at a heating rate of 10 °C/min.

The TG-DTG curves reveal that NC, NC/Cu-CD-MOF, and NC/Cu-CD-MOF-NPC materials all exhibit single-stage decomposition. As presented in Fig. S6, the TG-DTG curves of materials reveals a series of characteristic temperature values, encompassing the initial decomposition temperature (T_i), temperature of extrapolated onset (T_e), temperature of maximum pyrolysis rate (T_p), extrapolated end temperature (T_c), and final temperature (T_f). Upon comparing the degradation process of NC, the typical temperature points of NC were 179.5 °C, 197.2 °C, 206.9 °C, 219.9 °C, and 251.3 °C, respectively. It is evident that with the influence of Cu-CD-MOF, the typical temperature values of NC/Cu-CD-MOF are notably reduced to 178.2 °C, 195.6 °C, 206.0 °C, 221.9 °C, and 258.2 °C, respectively, which are 1.3 °C, 1.6 °C, and 0.9 °C lower than NC. Similarly, the addition of Cu-CD-MOF-NPC also reduces a series of typical temperatures of NC. The pyrolysis initiation temperature, extrapolation temperature, and peak temperature of NC/Cu-CD-MOF-NPC are 174.7 °C, 196.3 °C, and 206.7 °C, respectively, which are 4.8 °C, 0.9 °C, and 0.2 °C lower than NC. This alignment with earlier studies on NC pyrolysis signifies that the incorporation of catalysts leads to lower T_e and T_p values for the composite material compared to NC [57, 58], corroborated by DSC outcomes (Fig. 4d). The peak thermogravimetric temperature of NC/Cu-CD-MOF is 206.0 °C, which is 0.8 °C lower than the peak value of DSC. In addition, the peak thermogravimetric

temperature of NC/Cu-CD-MOF-NPC is 206.7 °C, which is 0.4 °C lower than the peak temperature of DSC. This discrepancy might stem from employing distinct instruments for the two evaluations [59]. The peak values of both are lower than the thermal decomposition peak values of pure NC, which decrease by 0.9 °C and 0.2 °C, respectively. In summary, both NC pyrolysis candidates can promote NC pyrolysis, where Cu-CD-MOF acts as a particularly effective catalyst, resulting in greater weight loss and a lower exothermic peak temperature. This is because of the porous structure, high specific surface area, and superior adsorption capacity of MOFs [60].

The mechanism of the thermal decomposition of NC materials has been extensively studied. Previous studies showed that the pyrolysis of NC begins with the breaking of the -O-NO₂ bond, which leads to NO₂ production. Then, the released NO₂ gas reacts with free radicals to generate other gaseous products, such as H₂O, CO₂, CO, NO, N₂O, NO₂, HCHO, and HCOOH [61].

The infrared characteristic absorption peaks of the gas-phase products produced by the thermal decomposition of NC are shown in **Table S6**. At typical temperature points (T_i , T_e , T_p , T_c , and T_f), the apparent changes in the infrared characteristic absorption peaks of gas decomposition products from NC, NC/Cu-CD-MOF and NC/Cu-CD-MOF-NPC are depicted in **Fig. 6** and **Table S7**. It is observed that during the decomposition process of NC with and without catalysts, detected gas products include H₂O, CO₂, CO, NO, N₂O, NO₂, HCHO, and HCOOH. Furthermore, the comparative study also considered gas generation at a specific temperature point T_x before the onset of decomposition temperature. It was found that the infrared absorption peaks of water and carbon dioxide remained unchanged at T_x and T_i , indicating that CO₂ and water are not the initial decomposition products of NC but originate from the environment.

At the initial decomposition temperature (T_i), the infrared absorption peaks of H₂O (3600–3740 cm⁻¹), CO₂ (2300–2360, 670 cm⁻¹), and NO₂ (1593–1635 cm⁻¹) are easily distinguishable for NC (**Fig. 6a**). As the temperature increases, additional gas species such as CO (2150–2195 cm⁻¹), NO (1763–1966 cm⁻¹), N₂O (2200–2300, 2241 cm⁻¹), HCHO (2700–2900 cm⁻¹), and HCOOH (1081–1129 cm⁻¹) are detected.

In the infrared absorption peaks of NC/Cu-CD-MOF at 165.3 °C (T_x) and 178.2 °C (T_i), distinct characteristic peaks of H₂O (3600–3740 cm⁻¹), CO₂ (2322–2376 cm⁻¹, 650 cm⁻¹), and NO₂ (1572–1643 cm⁻¹) can be observed (**Fig. 6b**). The decomposition results at these two temperatures differ from the initial stage of NC thermal decomposition, as NC does not decompose to produce NO₂ before the onset of the initial decomposition temperature. This also indicates the catalytic effect of Cu-CD-MOF. The peak observed at 3600–3740 cm⁻¹ can be attributed to the O—H bond stretching vibration of H₂O. The bands at 2322–2376 cm⁻¹ and 650 cm⁻¹ can be assigned to the stretching and bending vibration modes of CO₂, respectively. By comparing the infrared spectra under conditions of 165.3 °C (T_x) and 178.2 °C (T_i), it is observed that the intensities of H₂O, CO₂, and NO₂ remain almost unchanged. At 195.6 °C (T_e), the absorption peaks of H₂O, CO₂, and NO₂, and NO (1779–1963 cm⁻¹) are easily identifiable. As the temperature increases to T_p , the detection of NO, CO (2150–2190 cm⁻¹), N₂O (2200–2300, 2241 cm⁻¹), HCHO (2700–2900, 1720–1740 cm⁻¹), and HCOOH (1790, 1066–1132 cm⁻¹) is observed. The bands at 2700–2900 cm⁻¹ and 1720–1740 cm⁻¹ are related to the C—H and C = O stretching vibrations caused by the cleavage of the -CH₂ONO₂ group of HCHO [62]. The gas product of HCOOH is generated as a result of the secondary autocatalytic reaction of NC [63]. From the spectra, it can be observed that in the presence of Cu-CD-MOF, the gas intensities at the T_p temperature are significantly enhanced compared to the intensities at the adjacent temperatures (T_e and T_c). This confirms that the thermal decomposition rate of NC/Cu-CD-MOF composite is faster than that of pristine NC, indicating the catalytic effect of Cu-CD-MOF. At 221.9 °C (T_c), the intensities of N₂O, HCHO, and CO are weaker in the spectra compared to those at T_p . The increased intensities of NO, HCOOH, and H₂O could be attributed to residual

decomposition or catalytic reactions of NO₂ and HCHO [64]. In the final stage of decomposition, the peaks of HCOOH, NO, and CO disappear, while NO₂, CO₂, and H₂O can still be detected.

Using the Cu-CD-MOF-NPC catalyst, NC/Cu-CD-MOF-NPC detected gas products including H₂O, CO₂ and NO₂ in the infrared spectrum under T_x conditions (**Fig. 6c**). The H₂O, CO₂ and NO₂ infrared characteristic peaks were identified at the initial decomposition temperature T_i . At T_e , the intensity of the absorption peaks such as H₂O, CO₂ and NO₂ increased slightly, and the infrared characteristic peaks of NO (1770–1950 cm⁻¹) were detected. It can be seen that more gases are released at T_p , including H₂O, CO₂, NO₂, NO, N₂O (2200–2300 cm⁻¹), CO (2150–2194 cm⁻¹), HCHO (2700–2900 cm⁻¹), and HCOOH (1080–1120 cm⁻¹). At the temperature of T_c , the intensity of CO₂, HCOOH and H₂O increases, while the intensity of HCHO gas decreases, which is due to the reaction between HCHO gas and NO₂. Furthermore, distinguishable infrared bands of H₂O, CO₂ and NO₂ were detected at the final temperature T_f of the NC/Cu-CD-MOF-NPC decomposition process.

Fig. 6e shows a schematic diagram of the reaction mechanism of NC/Cu-CD-MOF. In the initial state, after the composite of NC and Cu-CD-MOF, Cu-CD-MOF plays an adsorption and catalytic role in the decomposition of NC through its unique porous structure. Specifically, during the decomposition process, the first thing that occurs is the breaking of the -O-NO₂ bond, releasing NO₂ gas. This is evidenced by a corresponding band change in FT-IR spectra (**Fig. 6b**, T_x). Due to the porous structure and high specific surface area of Cu-CD-MOF, it can adsorb the NO₂ gas produced by the first step of NC cracking, causing the gas product to remain in the polymer skeleton and subsequently leading to further breaking of the C—O-C bond, producing other products such as CO, CO₂, HCHO, and HCOOH. This is verified by the intensity distribution of gas-phase decomposition products in **Fig. 6b**. Similar to previous studies, Cu-CD-MOF not only accelerated the release of NO₂ from NC cracking but also further accelerated the decomposition process through self-catalytic reactions. This discovery provides a new perspective for understanding the decomposition mechanism of NC and a theoretical basis for developing efficient catalytic decomposition materials.

Through experimental analysis, NC/Cu-CD-MOF and NC/Cu-CD-MOF-NPC have demonstrated similar experimental results, indicating that they share the same reaction mechanism. Furthermore, the experimental data have confirmed the pivotal catalytic role of Cu-CD-MOF in the decomposition process of NC, providing robust support for its potential in practical applications. The significant effect of Cu-CD-MOF on the thermal decomposition of NC is mainly due to its porous structure (**Fig. S2**), high surface area (**Fig. S2**), and smaller particle size (**Fig. S7**). These attributes create conditions that allow Cu-CD-MOF to better enrich gases, thereby demonstrating superior catalytic activity. This is specifically manifested in the changes observed in the weight loss, exothermic peak temperature, and activation energy of the NC-based composite material.

Furthermore, it is noteworthy that the addition of Cu-CD-MOF and Cu-CD-MOF-NPC significantly reduces the emission of combustible and harmful gases compared to NC (**Fig. 6d&Fig. S8–9**). After adding Cu-CD-MOF, the intensity of CO decreased from 0.0115×10^{-3} to 5.13×10^{-3} , N₂O decreased from 0.0149×10^{-3} to 5.78×10^{-3} , and NO decreased from 0.0205×10^{-3} to 2.71×10^{-3} . Similarly, in NC/Cu-CD-MOF-NPC, the intensity of CO decreased to 5.39×10^{-3} , N₂O decreased to 5.73×10^{-3} , and NO decreased to 1.70×10^{-3} (**Table S8**). This is due to the direct carbonization of Cu-CD-MOF at high temperatures, resulting in the uniform-shaped Cu-CD-MOF to be disrupted and transformed into CD-MOF-derived carbon (CD-MOF-NPC) with an irregular porous structure (**Fig. S11d–f**). The porous CD-MOF and its residues provide space for the absorption of carbon oxides and nitrogen oxides.

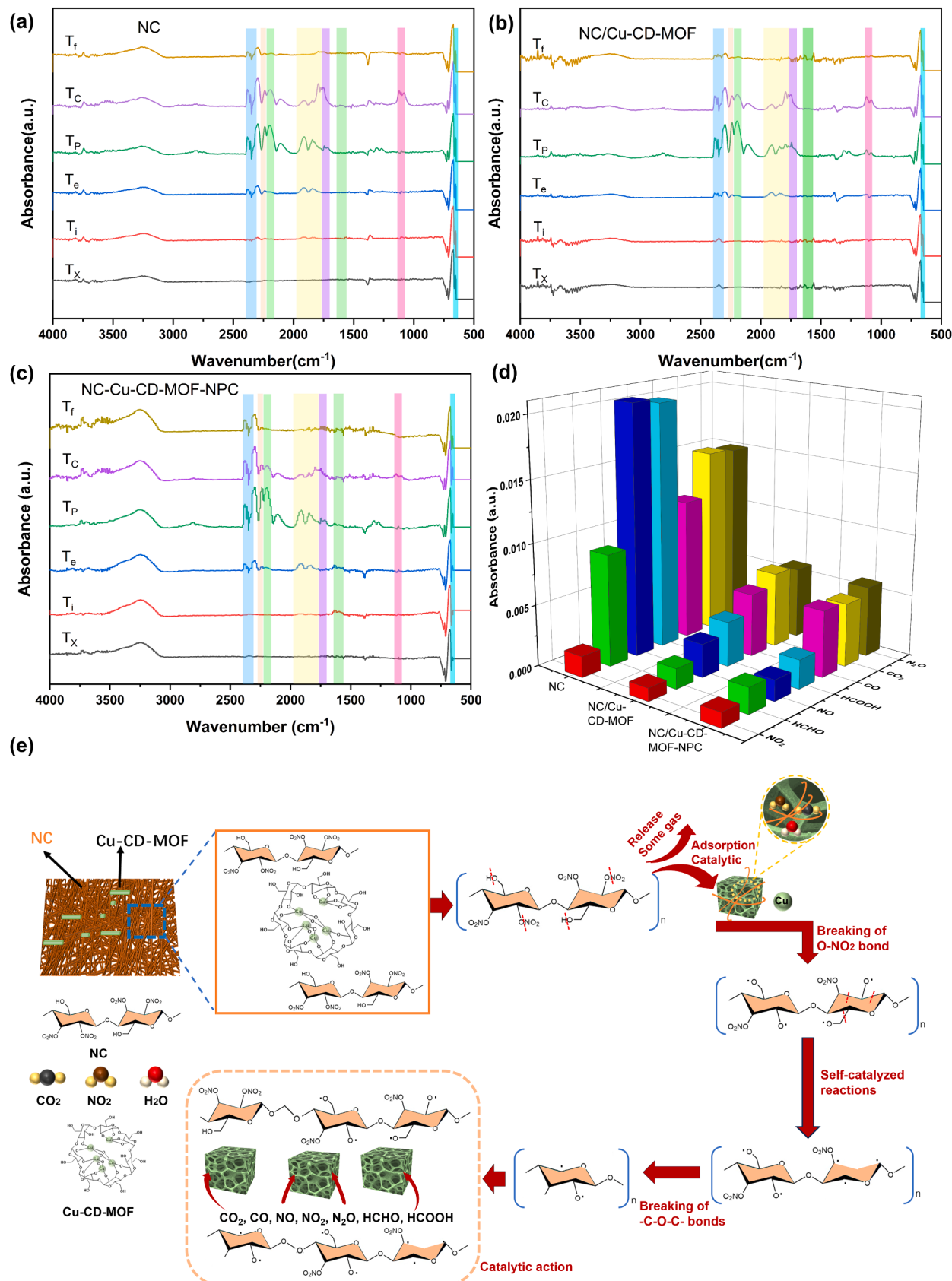


Fig. 6. FT-IR spectra of the gases evolved from the degradation of NC (a) and NC/Cu-CD-MOF (b) and NC-Cu-CD-MOF-NPC (c). (d) The intensity distribution of gas-phase decomposition products. (e) Schematic diagram of the reaction mechanism of NC/Cu-CD-MOF.

4. Conclusion

In this work, Cu-CD-MOF and Cu-CD-MOF-NPC were confirmed to possess an effective thermal catalytic activity and exhibit good compatibility with NC. It was demonstrated that, as promising green catalysts, Cu-CD-MOF and Cu-CD-MOF-NPC can help NC overcome the energy barrier. The activation energies of the NC/Cu-CD-MOF and NC/Cu-CD-MOF-NPC composite materials decreased by 21.5 kJ/mol and 19.7 kJ/mol respectively, compared to NC alone. TG-FTIR analysis confirmed that the pyrolysis processes of the NC/Cu-CD-MOF and NC/Cu-CD-MOF-NPC complexes differ from that of pristine NC. Both NC/Cu-CD-MOF and NC/Cu-CD-MOF-NPC facilitate the $-O-NO_2$ bond breaking during the initial stage of NC thermolysis and the condensed-phase decomposition. Besides, the emission of combustible and harmful gases (CO, NO, N₂O, NO₂) was reduced, due to the porous structure, high surface area, and smaller particle size of Cu-CD-MOF and Cu-CD-MOF-NPC.

CRediT authorship contribution statement

Yameng Chai: Writing – review & editing, Writing – original draft, Visualization, Methodology, Investigation, Formal analysis, Data curation, Conceptualization. **Wenjia Li:** Writing – review & editing, Validation, Software, Investigation, Data curation. **Fuqiang Du:** Resources, Validation, Writing – review & editing. **Jianchun Zhao:** Validation, Writing – review & editing. **Shiyiing Li:** Writing – review & editing, Validation, Supervision. **Yajun Ding:** Writing – review & editing, Supervision, Resources, Project administration, Conceptualization. **Sanjiu Ying:** Project administration, Funding acquisition, Conceptualization. **Jie Zhou:** Writing – review & editing, Supervision, Resources, Project administration, Conceptualization.

Declaration of competing interest

The authors declare that they have no known competing financial interests or personal relationships that could have appeared to influence the work reported in this paper.

Data availability

Data will be made available on request.

Acknowledgments

The authors thank the Priority Academic Program Development (PAPD) of Jiangsu Higher Education Institutions.

Supplementary materials

Supplementary material associated with this article can be found, in the online version, at [doi:10.1016/j.polymdegradstab.2024.110958](https://doi.org/10.1016/j.polymdegradstab.2024.110958).

References

- [1] J. Yoon, J. Lee, B. Choi, D. Lee, D.H. Kim, D.M. Kim, Dong-II Moon, Flammable carbon nanotube transistors on a nitrocellulose paper substrate for transient electronics, *Nano Res* 10 (1) (2017) 87–96.
- [2] X. Yang, Y. Wang, Y. Li, Z. Li, T. Song, X. Liu, J. Hao, Thermal stability and mechanical properties of hybrid materials based on nitrocellulose grafted by aminopropylisobutyl polyhedral oligomeric silsesquioxane, *Polimery* 62 (7-8) (2017) 576–587.
- [3] A.F. Tarchoun, D. Trache, T.M. Klapötke, S. Chelouche, M. Derradji, W. Bessa, A. Mezroua, A promising energetic polymer from *positidonia oceanica* brown algae: synthesis, characterization, and kinetic modeling, *Macromol. Chem. Phys.* 220 (22) (2019) 1900358.
- [4] L. Chen, X. Mao, Q. Li, X. Cao, J. Zhang, Y. Wang, J. Liu, W. He, One-step, safe and efficient preparation strategy of nitrate glycerol ether cellulose-based energetic composites with application potential in propellants, *Compos. Commun.* 28 (2021) 100956.
- [5] M. Dourari, A.F. Tarchoun, D. Trache, A. Abdelaziz, T. Barkat, R. Tiliouine, S. Bekhouche, W. Bessa, Elucidating the effect of nitrocellulose-encapsulated MgAl-CuO on the thermal behavior of double base propellant based on nitrocellulose and diethylene glycol dinitrate, *React. Kinet., Mech. Catal.* 136 (4) (2023) 2309–2325.
- [6] W.Q. Pang, X. Xia, Y. Zhao, D. Trache, L.T. DeLuca, S.Q. Meng, X.G. Liu, H.J. Yu, Effect of carbon nanotubes (CNTs) on the performance of solid rocket propellants (SRPs): a short review, *FirePhysChem* 3 (3) (2023) 227–233.
- [7] N. Matmat, A. Abdelaziz, D. Trache, A.F. Tarchoun, H. Boukeciat, A. Rahal, Elaboration, spectroscopic characterization, and study of the thermal decomposition process of energetic composites based on ammonium perchlorate and dual-biopolymers, *FirePhysChem* 4 (2) (2024) 166–176.
- [8] S. Bekhouche, D. Trache, H. Akbi, A. Abdelaziz, A.F. Tarchoun, H. Boudouh, Thermal decomposition behavior and kinetic study of nitrocellulose in presence of ternary nanothermites with different oxidizers, *FirePhysChem* 3 (3) (2023) 208–216.
- [9] D. Trache, A.F. Tarchoun, Stabilizers for nitrate ester-based energetic materials and their mechanism of action: a state-of-the-art review, *J. Mater. Sci.* 53 (1) (2017) 100–123.
- [10] W. Qu, S. Niu, D. Sun, H. Gao, Y. Wu, Z. Yuan, X. Chen, Y. Wang, T. An, G. Wang, F. Zhao, Pb single atoms enable unprecedented catalytic behavior for the combustion of energetic materials, *Adv. Sci.* 8 (5) (2021) 2002889.
- [11] H. ZHANG, T. AN, F. ZHAO, X. ZHANG, J. YI, S. XU, Preparation of zirconium/copper gallate and its effect on combustion of double-base and RDX-CMDB propellants, *Acta Armamentarii* 34 (6) (2013) 690.
- [12] W.Q. Pang, L.T. DeLuca, X.Z. Fan, O.G. Glotov, K. Wang, Z. Qin, F.Q. Zhao, Combustion behavior of AP/HTPB/Al composite propellant containing hydroborate iron compound, *Combust. Flame*, 220 (2020) 157–167.
- [13] D.R. Kshirsagar, S. Jain, S.N. Jawalkar, N.H. Naik, S. Pawar, M. Maurya, Evaluation of nano-Co₃O₄ in HTPB-based composite propellant formulations, *Propellants, Explos., Pyrotech* 41 (2) (2016) 304–311.
- [14] M.H. Yap, K.L. Fow, G.Z. Chen, Synthesis and applications of MOF-derived porous nanostructures-sciencedirect, *Green Energy Environ* 2 (3) (2017) 218–245.
- [15] L. Lu, J. Wang, C. Shi, Y. Sun, W. Wu, Y. Pan, M. Muddassir, Four structural diversity MOF-photocatalysts readily prepared for the degradation of the methyl violet dye under UV-visible light, *New J. Chem.* 45 (2) (2021) 551–560.
- [16] T.A. Goetjen, J. Liu, Y. Wu, J. Sui, X. Zhang, J.T. Hupp, O.K. Farha, Metal-organic framework (MOF) materials as polymerization catalysts: a review and recent advances, *Chem. Commun.* 56 (72) (2020) 10409–10418.
- [17] J.J. Du, X. Zhang, X.P. Zhou, D. Li, Robust heterometallic MOF catalysts for cyanosilylation of aldehydes, *Inorg. Chem. Front.* 5 (11) (2018) 2772–2776.
- [18] Y.Z. Chen, R. Zhang, L. Jiao, H.L. Jiang, Metal-organic framework-derived porous materials for catalysis, *Coordin. Chem. Rev.* 362 (2018) 1–23.
- [19] S. Wang, B. Ye, C. An, J. Wang, Q. Li, Synergistic effects between Cu metal-organic framework (Cu-MOF) and carbon nanomaterials for the catalysis of the thermal decomposition of ammonium perchlorate (AP), *J. Mater. Sci.* 54 (6) (2019) 4928–4941.
- [20] Q. Yang, G. Yang, W. Zhang, S. Zhang, Z. Yang, G. Xie, Q. Wei, S. Chen, S. Gao, Superior thermostability, good detonation properties, insensitivity, and the effect on the thermal decomposition of ammonium perchlorate for a new solvent-free 3D energetic PbII-MOF, *Chem-Eur. J.* 23 (38) (2017) 9149–9155.
- [21] Y. Yang, Y. Bai, F. Zhao, E. Yao, J. Yi, C. Xuan, S. Chen, Effects of metal organic framework Fe-BTC on the thermal decomposition of ammonium perchlorate, *RSC Adv* 6 (71) (2016) 67308–67314.
- [22] I. Roy, J.F. Stoddart, Cyclodextrin metal-organic frameworks and their applications, *Acc. Chem. Res.* 54 (6) (2021) 1440–1453.
- [23] L. Xu, D. Ke, L. Chen, Z.J. Qiu, S.L. Zeng, B.J. Li, S. Zhang, Amino-functionalized β -Cyclodextrin to construct green metal-organic framework materials for CO₂ capture, *ACS Appl. Mater. Interfaces*, 12 (2) (2019) 3032–3041.
- [24] S.V. Dummitt, H. Saini, M.Z. Hussain, K. Yadava, K. Jayaramulu, A. Casini, R. A. Fischer, Cyclodextrin metal-organic frameworks and derivatives: recent developments and applications, *Chem. Soc. Rev.* 51 (12) (2022) 5175–5213.
- [25] J.F. Feng, M. Tan, S. Zhang, B.J. Li, Recent advances of porous materials based on cyclodextrin, *Macromol. Rapid Commun.* 42 (23) (2021) 2100497.
- [26] A. Shahzaib, I. Ahmad, P. Singh, F. Zafar, Y. Akhtar, A.A. Bukhari, N. Nishat, Ultrarapid and highly efficient reduction of nitroaromatic compounds using cyclodextrin MOF, *Catal. Commun.* 174 (2023) 106569.
- [27] J. Szejtli, ChemInform abstract: introduction and general overview of cyclodextrin chemistry, *ChemInform* 29 (39) (2010).
- [28] T. Volkova, A. Surov, I. Terekhova, Metal-organic frameworks based on β -cyclodextrin: design and selective entrainment of non-steroidal anti-inflammatory drugs, *J. Mater. Sci.* 55 (27) (2020) 13193–13205.
- [29] C.S. Do Carmo, C. Maia, J. Poejo, I. Lychko, P. Gamito, I. Nogueira, M.R. Bronze, A. T. Serra, Microencapsulation of α -tocopherol with zein and β -cyclodextrin using spray drying for colour stability and shelf-life improvement of fruit beverages, *RSC Adv* 7 (51) (2017) 32065–32075.
- [30] M.P. Abuçay, B.L. Caetano, B.G. Chiari-Andréo, B. Fonseca-Santos, A.M. do Santos, M. Chorilli, L.A. Chiavacci, Supramolecular cyclodextrin-based metal-organic frameworks as efficient carrier for anti-inflammatory drugs, *Eur. J. Pharm. Biopharm.* 127 (2018) 112–119.
- [31] W. Jiang, H. Liu, Q. Liao, T. Tang, J. Liu, Z. Liu, J. Yan, Preparation of two metal organic frameworks (K - β -CD-MOFs and Cs- β -CD-MOFs) and the adsorption research of myricetin, *Polyhedron* 196 (2021) 114983.
- [32] W. Li, Y. Gan, Y. Li, S. Li, J. Liang, W. Fan, Z. Yu, Y. Li, Y. Ding, Z. Xiao, J. Zhou, Enhancing propellant performance through intermolecular interactions:

- cyclodextrin-based MOF loading in nitrocellulose, *Phys. Chem. Chem. Phys.* 25 (42) (2023) 29201–29210.
- [33] N.A. Surib, A. Kuila, P. Saravanan, L.C. Sim, K.H. Leong, A ligand strategic approach with Cu-MOF for enhanced solar light photocatalysis, *New J. Chem.* 42 (13) (2018) 11124–11130.
- [34] S. Wang, G. Shao, H. Zhao, L. Yang, L. Zhu, H. Liu, B. Cui, D. Zhu, J. Li, Y. He, Covering soy polysaccharides gel on the surface of β -cyclodextrin-based metal-organic frameworks, *J. Mater. Sci.* 56 (4) (2020) 3049–3061.
- [35] Y. Xiao, J. Thomas, N.T. Nguyen, T.T. Le, C.T. Chang, Study on removal of volatile organic compounds by metal-organic framework composite material. 2021.
- [36] C. Qiu, J. Wang, Y. Qin, H. Fan, X. Xu, Z. Jin, Green synthesis of cyclodextrin-based Metal-Organic frameworks through the seed-mediated method for the encapsulation of hydrophobic molecules, *J. Agric. Food Chem.* 66 (16) (2018) 4244–4250.
- [37] C. Qiu, J. Wang, Y. Qin, H. Fan, X. Xu, Z. Jin, Novel approach with controlled nucleation and growth for green synthesis of size-controlled cyclodextrin-based metal-organic frameworks based on short-chain starch nanoparticles, *J. Agric. Food Chem.* 66 (37) (2018) 9785–9793.
- [38] Z. Hu, S. Li, S. Wang, B. Zhang, Q. Huang, Encapsulation of menthol into cyclodextrin metal-organic frameworks: preparation, structure characterization and evaluation of complexing capacity, *Food Chem.* 338 (2021) 127839.
- [39] I. Shown, S. Banerjee, A.V. Ramchandran, K.E. Geckeler, C.N. Murthy, Synthesis of cyclodextrin and sugar-based oligomers for the efavirenz drug delivery, *Macromol. Symp.* 287 (1) (2010) 51–59.
- [40] N. Marangoci, M. Mares, M. Silion, A. Fifere, C. Varganici, A. Nicolescu, C. Deleanu, A. Coroaba, M. Pintea, B.C. Simionescu, Inclusion complex of a new propiconazole derivative with β -cyclodextrin: NMR, ESI-MS and preliminary pharmacological studies, *Results Pharma Sci* 1 (1) (2011) 27–37.
- [41] P. Singla, R. Kumar, P.K. Soni, S.C. Sahoo, A. Singh, Chemical compatibility of energetic metal complexes with polymers by thermal analytical techniques, *FirePhysChem* (2024).
- [42] A.F. Tarchoun, D. Trache, M.A. Hamouche, A. Abdelaziz, S. Chelouche, H. Boukeciat, T.M. Klapötke, New insights into the chemical compatibility of nitrochitosan with potential energetic molecules, *Processes* 11 (11) (2023) 3060.
- [43] C.K. Pu, M.J. Yi, Y. Luan, Z.G. Xiao, A balanced strategy for energy level, mechanical properties and sensitivity of the gun propellants based on step ladder-structured nitrocellulose, *Cellulose* 30 (4) (2023) 2367–2384.
- [44] T. AN, F. ZHAO, H. GAO, H. MA, H. HAO, J. YI, Y. YANG, Preparation of super thermites and their compatibilities with db propellants components, *J. Mater. Eng.* 1 (11) (2011) 23–28.
- [45] Y. Guo, N. Zhao, T. Zhang, H. Gong, H. Ma, T. An, F. Zhao, R. Hu, Compatibility and thermal decomposition mechanism of nitrocellulose/Cr₂O₃ nanoparticles studied using DSC and TG-FTIR, *RSC Adv* 9 (7) (2019) 3927–3937.
- [46] A. Benhammada, D. Trache, M. Kesraoui, S. Chelouche, Hydrothermal synthesis of hematite nanoparticles decorated on carbon mesospheres and their synergistic action on the thermal decomposition of nitrocellulose, *Nanomateri* 10 (5) (2020) 968.
- [47] A. Benhammada, D. Trache, M. Kesraoui, A.F. Tarchoun, S. Chelouche, A. Mezroua, Synthesis and characterization of α -Fe₂O₃ nanoparticles from different precursors and their catalytic effect on the thermal decomposition of nitrocellulose, *Thermochim. Acta* 686 (2020) 178570.
- [48] A. Benhammada, D. Trache, S. Chelouche, Catalytic effect investigation of α -Fe₂O₃ and α -Fe₂O₃-CMS nanocomposites on the thermal behavior of NC/DEGDN mixture: DSC measurements and kinetic modeling, *J. Indian Chem. Soc.* 100 (1) (2023) 100838.
- [49] E.K.C. Moens, K.D. Smit, Y.W. Marien, A.D. Trigilio, P.H.M. Van Steenberge, K. M. Van Geem, J.L. Dubois, D.R. D'hooge, Progress in reaction mechanisms and reactor technologies for thermochemical recycling of poly(methyl methacrylate), *Polymers* 12 (8) (2020) 1667.
- [50] N. Zhao, E. Yao, H. Ma, J. Zeng, Z. Yu, T. An, F. Zhao, X. Yu, Studies on thermokinetic and reactive mechanism of graphdiyne-based NC composite via multi isoconversional methods and model reconstruction, *Cellulose* 29 (8) (2022) 4365–4379.
- [51] P.E. Sánchez-Jiménez, L.A. Pérez-Maqueda, A. Perejón, J.M. Criado, A new model for the kinetic analysis of thermal degradation of polymers driven by random scission, *Polym. Degrad. Stab.* 95 (5) (2010) 733–739.
- [52] N. Zhao, H. Ma, E. Yao, Z. Yu, T. An, F. Zhao, X. Yu, Influence of tailored CuO and Al/CuO nanothermites on the thermocatalytic degradation of nitrocellulose and combustion performance of AP/HTPB composite propellant, *Cellulose* 28 (13) (2021) 8671–8691.
- [53] V. Mamleev, S. Bourbigot, M.L. Bras, J. Lefebvre, Three model-free methods for calculation of activation energy in TG, *J. Therm. Anal. Calorim.* 78 (2004) 1009–1027.
- [54] S.A. Hadigheh, Y. Wei, S. Kashi, Optimisation of CFRP composite recycling process based on energy consumption, kinetic behaviour and thermal degradation mechanism of recycled carbon fibre, *J. Cleaner Prod.* 292 (2021) 125994.
- [55] M. Rajic, M. Suceska, Influence of ageing on nitrocellulose thermal properties and hazard potential figures-of-merit, *High Temp-High Press* 32 (2) (2000) 171–178.
- [56] A. Benhammada, D. Trache, Thermal decomposition of energetic materials using TG-FTIR and TG-MS: a state-of-the-art review, *Appl. Spectrosc. Rev.* 55 (8) (2020) 724–777.
- [57] N. Zhao, J. Li, F. Zhao, T. An, R. Hu, H. Ma, Combustion catalyst: nano-Fe₂O₃ and nano-thermite Al/Fe₂O₃ with different shapes, *Dev. Combust. Technol.* 325 (2016).
- [58] S. Bekhouche, D. Trache, A. Abdelaziz, A.F. Tarchoun, S. Chelouche, A. Boudjellal, A. Mezroua, Preparation and characterization of MgAl-CuO ternary nanothermite system by arrested reactive milling and its effect on the thermocatalytic decomposition of cellulose nitrate, *Chem. Eng. J.* 453 (2023) 139845.
- [59] N. Zhao, J. Li, H. Gong, T. An, F. Zhao, A. Yang, R. Hu, H. Ma, Effects of α -Fe₂O₃ nanoparticles on the thermal behavior and non-isothermal decomposition kinetics of nitrocellulose, *J. Anal. Appl. Pyrolysis*. 120 (2016) 165–173.
- [60] N. Zhao, Z. Yu, H. Ma, E. Yao, T. An, F. Zhao, X. Yu, Fe₂O₃/ZIF-8 architectures with enhanced thermocatalytic performance for efficient degradation of nitrocellulose, *J. Phys. Chem. Solids*. 174 (2023) 111186.
- [61] X. Gao, L. Jiang, Q. Xu, Experimental and theoretical study on thermal kinetics and reactive mechanism of nitrocellulose pyrolysis by traditional multi kinetics and modeling reconstruction, *J. Hazard. Mater.* 386 (2020) 121645.
- [62] A. Gratien, E. Nilsson, J.F. Doussin, M.S. Johnson, C.J. Nielsen, Y. Stenström, B. Picquet-Varrault, UV and IR absorption cross-sections of HCHO, HCDO, and DCDO, *J. Phys. Chem. A* 111 (45) (2007) 11506–11513.
- [63] A.B. Shehata, M.A. Hassan, M.A. Nour, Effect of new poly 2-acryloyl-N,N'-bis (4-nitrophenyl) propan diamide and poly 2-acryloyl-N,N'-bis (4-methylphenyl) propan diamide and their synergistic action on the stability of nitrocellulose, *J. Hazard. Mater.* 102 (2-3) (2003) 121–136.
- [64] W. Wei, B. Cui, X. Jiang, L. Lu, The catalytic effect of NiO on thermal decomposition of nitrocellulose, *J. Therm. Anal. Calorim.* 102 (3) (2010) 863–866.